http://dx.doi.org/10.5012/bkcs.2013.34.8.2343

# Electrochemical Performance of Activated Carbons/$Mn_3O_4$-Carbon Blacks for Supercapacitor Electrodes

**Ki-Seok Kim and Soo-Jin Park***

*Department of Chemistry, Inha University, Incheon 402-751, Korea. *E-mail: sjpark@inha.ac.kr*
*Received February 26, 2013, Accepted May 14, 2013*

In this work, manganese dioxide ($Mn_3O_4$)/carbon black (CB) composites (Mn-CBs) were prepared by an *in situ* coating method as electrical fillers and the effect of the Mn-CBs on the electrical performance of activated carbon (AC)-based electrodes was investigated. Structural features of Mn-CBs produced *via in situ* coating using a $KMnO_4$ solution were confirmed by XRD and TEM images. The electrical performances, including cv curves, charge-discharge behaviors, and specific capacitance of the ACs/Mn-CBs, were determined by cyclic voltammograms. It was found that the composites of $Mn_3O_4$ and CBs were successfully formed by *in situ* coating method. ACs/Mn-CBs showed higher electrical performance than that of AC electrodes fabricated with conventional CBs due to the pesudocapacitance reaction of manganese oxides in the aqueous electrolyte. Consequently, it is anticipated that the incorporation of $Mn_3O_4$ into CBs could facilitate the utilization of CBs as electrical filler, leading to enhanced electrochemical performance of AC electrodes for supercapacitors.

**Key Words :** Supercapacitors, Manganese dioxide, Carbon blacks, Activated carbons, Electrochemical performances

## Introduction

Recently, supercapacitors, also called electrochemical capacitors (ECs) or ultracapacitors, are an energy storage system with unique characteristics, such as high power and power density and long cycle life compared to electrical double-layer capacitors. With these advantages, the demand of supercapacitors is increased with fast-growing the portable electronic devices and hybrid electric vehicles (HEVs). Thus, for an advanced supercapacitor, the active electrode materials with high capacity performance have been studied by many researchers.[1-4]

The supercapacitors are generally classified as following three categories: conductive polymer, transition metal, and carbon materials. Aiming for a carbon electric double layer capacitor (EDLC) of low cost, activated carbon (ACs)-based electrodes are the most developed technology because of their low cost, high surface area, good electrical conductivity and excellent chemical stability, large capacitance, and long cycling life. Electrostatic charges are stored at the ACs/electrolyte double layer interface and there is no faradic reaction. Also, to optimize the cost and electrochemical performance of EDLCs, the present work focuses on carbon combination electrodes that contain AC as the main source for providing high capacitance and carbon blacks (CBs), carbon nanotubes (CNTs), and carbon nanofibers (CNFs) as the conductive additive and CBs is mainly used as conductive additive. As well-known, the electrochemical performance of AC-based electrodes is strongly affected by the property of conductive additives and effects of conductive additive on electrochemical performance of EDLCs have been fully studied.[5-8]

Nowadays, to provide pseudocapacitance to carbon material-based electrodes, the incorporation of the metal oxide materials, such as RuO, NiO, $IrO_2$, $Co_3O_4$, and $MnO_2$ to carbon materials have been studied extensively. Among these metal oxides, amorphous hydrated ruthenium oxide ($RuO_2$) has been found to be its ideal pseudocapacitive behaviors (high specific capacitance of over 700 F/g) and good reversibility. However, the high cost of the $RuO_2$ is the most disadvantages for its practical applications. Thus, the substitutes of $RuO_2$ have attracted much attention. Recently, manganese dioxides are promising supercapacitor materials due to the low cost of raw materials, natural abundance, rich redox behaviors, environmentally friendlier than other transition metal oxide materials, and non-toxicity criteria and high performance.[9-11]

To take benefit from the electrochemical performance of ACs and improved electrical properties of CBs in supercapacitors, the incorporation of the $Mn_3O_4$ to the activated carbon/CB-based active materials is the aim of this paper. Therefore, in this present work, carbon blacks as electrical filler were mixed with $Mn_3O_4$ *via in situ* coating method. The effect of $Mn_3O_4$/carbon black composites on electrochemical performances, such as CV-curves, charge-discharge behaviors, and specific capacitance of activated carbon-based electrodes is discussed.

## Material and Methods

**Materials.** The activated carbons (ACs) were supplied from Kuraray Chem. (Surface area: 1700-1800 $m^2/g$, Japan). Carbon blacks (CBs, Hi Black 420B) were supplied from Korea Carbon Black (Korea). Potassium permanganate ($KMnO_4$) was supplied from Sam Chum Chem (Korea). The citric acid and all other organic solvents used in this study

were of analytical grade and used without further purification.

**Preparation of $Mn_3O_4$/Carbon Black Composites.** 1.0 g of pristine carbon blacks was mixed with 100 mL of 0.1, 0.2, and 0.3 M $KMnO_4$ solution in the flask. The mixture solution was then refluxed at 140 °C with stirring for 12 h. After reaction, the mixture was filtered and washed with distilled water several times to remove the residual $KMnO_4$. Subsequently, the filter cake was redispersed in 200 mL of deionized water and 10 mL of 1 M citric acid solution was added dropwise with the temperature of the oil bath maintained at 160 °C for 12 h, under vigorous magnetic stirring during the whole course. A condenser was fitted to the reactor to prevent liquid loss by evaporation. Finally, the composite products were obtained through filtering, washing with water, and drying processes. The prepared samples were named Mn1-CBs, Mn2-CBs, and Mn3-CBs.

**Characterization.** The surface morphologies of carbon blacks (CBs) and $Mn_3O_4$/carbon blacks composites (Mn-CBs) were observed by transmission electron microscopy (TEM, JEOL FE-TEM 2006) and the content of manganese was examined using Inductive Coupled Plasma-Mass Spectrometer (ICP-MS, ELAN 6100).

The thermal properties of CBs and Mn-CBs were measured using thermogravimetric analyses (TGA, Du-Pont TGA-2950 analyzer) from 30 to 900 °C at a heating rate of 10 °C/min in a nitrogen atmosphere.

The structures of the CBs and Mn-CBs were determined by X-ray diffraction (XRD, Rigaku D/Max 2200V) at 40 kV and 40 mA using Cu Kα radiation. The XRD patterns were obtained in 2θ ranges between 2° and 70° at a scanning rate of 2°/min.

Electrochemical properties of the ACs/CBs and ACs/Mn-CBs were characterized using a three electrode electrochemical cell. The three-electrode cell consisted of a Pt wire as a counter electrode, an Ag/AgCl reference electrode, and Ni foam coated with samples as the working electrode. To obtain the working electrode, the ACa, Mn-CBs, and PVDF (70:20:10, w/w) were mixed in NMP. The slurry mixture was then coated onto Ni foam, which was dried at 100 °C for 12 h. The coating weight was fixed about 5 mg. Cyclic voltammetry measurements were carried out on an Ivium-Stat instrument in 0.5 M $Na_2SO_4$ solution at scan rates of 5, 10, 20, 30, and 50 mV/s in a voltage range 0 to 0.8 V. Galvanostatic charge/discharge curves were measured at different current densities from 0.1 to 1 A/g.

## Results and Discussion

Figure 1 shows TEM images to obtain visualization of the diameter and surface features of pristine CBs and Mn-CBs. It can be seen that pure CBs which have a diameter of about 40 nm exhibit spherical form and a randomly aggregated structure, as shown in Figure 1(a). However, CBs were more aggregated after $Mn_3O_4$ coating and the diameter (about 60 nm) of the CBs is slightly increased (Fig. 1(b)). Moreover, the Mn-CBs present the rough surface compared to pristine

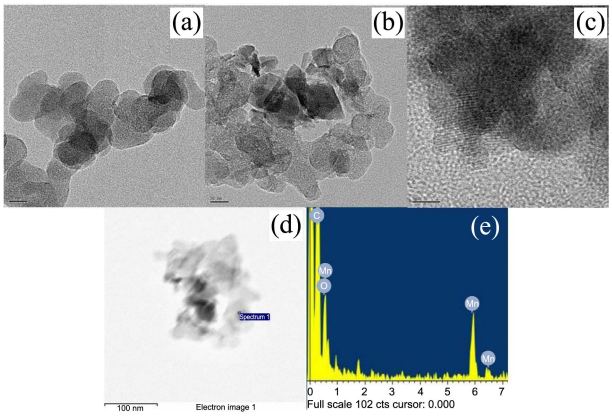


**Figure 1.** TEM images of (a) pristine CBs, (b) Mn-CB, and (c, d) EDS images of Mn-CBs.

**Table 1.** Manganese content of Mn-CBs prepared with different $KMnO_4$ concentrations

| Sample | Content (%) |
|---|---|
| CBs | - |
| Mn1-CBs | 19.9 |
| Mn2-CBs | 33.7 |
| Mn3-CBs | 53.1 |

CBs, indicating successful forming $Mn_3O_4$/CB composites. The Figure 1(c) showed the crystal lattice fringes throughout the $Mn_3O_4$ formed on CBs. The Mn-CBs are further confirmed by EDX image (Fig. 1(d) and (e)). It indicates that Mn-CBs are consisted of three main peaks, such as carbon, oxygen, and manganese. Also, the content of manganese in the Mn-CBs samples increase with increasing $KMnO_4$ concentration, as shown in Table 1.

TGA thermogram of pristine CBs and Mn-CBs are shown in Figure 2. It is clear that CBs exhibit higher thermal stability (weight loss, about 4%) of up to 900 °C with partial weight loss. However, the thermogram of Mn-CBs is visibly different. Mn-CBs exhibit a gradual weight loss (9%) up to 535 °C, and then the total weight loss with second degradation is about 16%. It means that the oxygen of $Mn_3O_4$ was

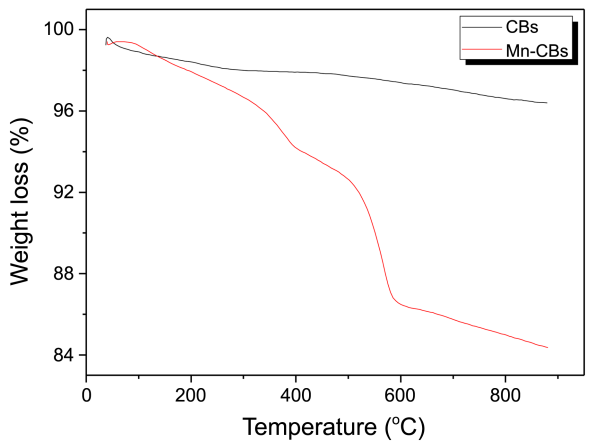


**Figure 2.** TGA thermograms of pristine CBs and Mn-CB.

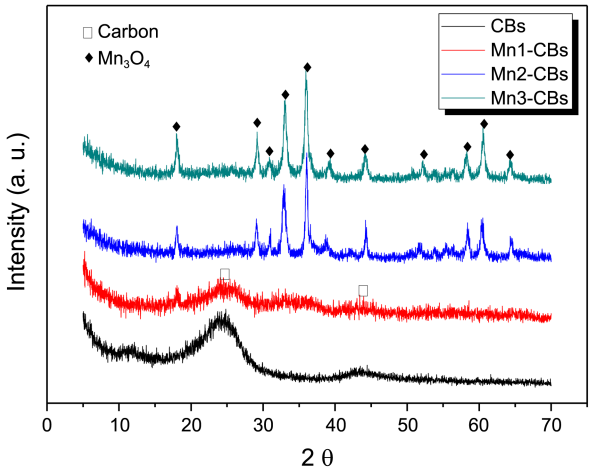


**Figure 3.** XRD patterns of pristine CBs and Mn-CBs with different $Mn_3O_4$ content.

evaporated over 535 °C, resulting in the formation of $Mn_3O_4$ of low oxidized state.[12]

Figure 3 shows the XRD patterns of the pristine CBs and Mn-CBs. As expected, the pristine CBs revealed reflections corresponding to the weak d(002) and d(100) planes of crystalline graphite-like materials at 2θ = 26 and 43, respectively. In Mn-CBs, three peaks are detected at 2θ = 18°, 29°, 31°, 33°, 36°, 39°, 44°, 52°, 58°, 60°, and 64°, corresponding to d(101), d(112), d(200), d(103), d(211), d(004), d(220), d(105), d(321), d(224) and d(314) of $Mn_3O_4$ mixed onto carbon blacks. In addition, the intensity of the main peaks of $Mn_3O_4$ increases with increasing $KMnO_4$ concentration. In the case of the 0.1 M $Mn_3O_4$-CBs, there are no significant changes of the XRD peaks compared to pristine CBs, although some changes are locally shown. However, the peak intensity of $Mn_3O_4$ increases above 0.1 M $KMnO_4$, indicating the formation of uniform $Mn_3O_4$/CB composites.[13]

Figure 4 shows the cyclic voltammogram of ACs/CBs and ACs/Mn-CB electrodes with different $Mn_3O_4$ concentrations, measured at 10 mV/s in a 0.5 M $Na_2SO_4$ solution as an electrolyte. As shown in Figure 4(a), the CV curve has a rectangular shape and symmetric current-potential characteristics between 0 and 0.8 V, indicating excellent capacitive behaviors through the 0.8 V voltage window in the $Na_2SO_4$ electrolyte solution. ACs/Mn-CBs electrodes exhibit larger current density compared to ACs/CBs, indicating the higher specific capacitance of ACs/Mn-CB. In addition, the current density of the ACs/Mn-CB electrodes increases with increasing $Mn_3O_4$ concentration. These results indicate that the incorporation of $Mn_3O_4$ layers onto CBs can increase the electrochemical utilization of conventional CBs as electrical filler.

Figure 4(b) shows CV curves of ACs/Mn3-CB as a function of different scan rates from 5 to 50 mV/s. It can be found that the cathodic peaks and anodic peaks shift in the positive and negative directions, respectively, which is attributed to the resistance of the electrodes. The increase of the current of the ACs/Mn3-CBs with different scan rates exhibits the rapid rate capability of the electrodes.[14] However, as the scan rate is increased, the current density of the CV curves is depressed, suggesting that the scan rate is affected to the efficiency of ion transport into the carbon electrodes.

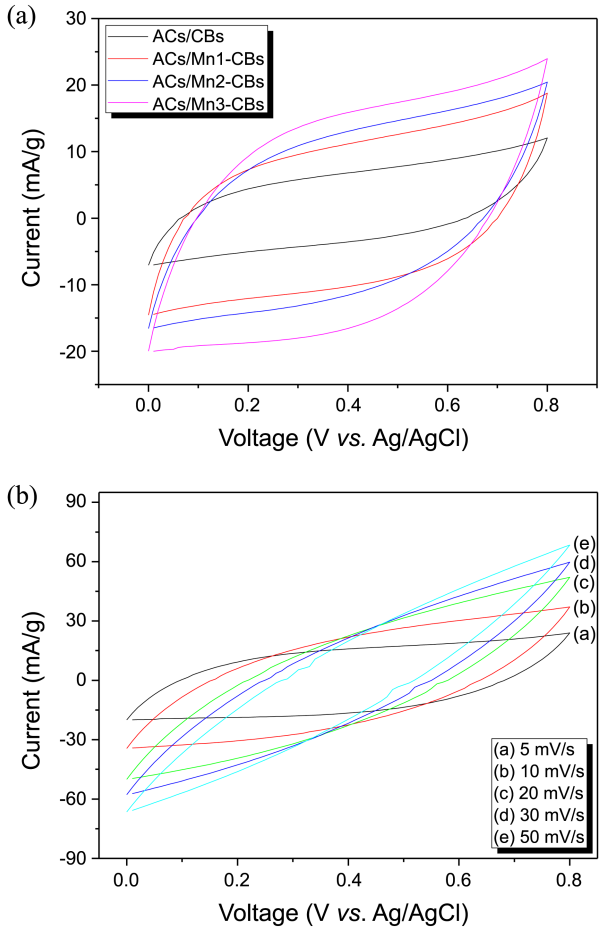


**Figure 4.** Cyclic voltammetry of (a) ACs/CBs and ACs/Mn-CBs with different $Mn_3O_4$ content at 10 mV/s scan rate and (b) ACs/Mn3-CBs with different scan rates from 5 to 50 mV/s.

Figure 5 shows the galvanostatic charge/discharge curve of ACs/CBs and ACs/Mn-CB electrodes with different $Mn_3O_4$ concentrations. It can be found that the charge-discharge duration increases as the concentration of $Mn_3O_4$ mixed onto CBs rises, as shown in Figure 5(a). Also, the charge voltage becomes lower and the discharge voltage becomes higher with the incorporation of a $Mn_3O_4$ layer onto the CBs, indicating an increase of the energy storage capacity by a reduction of the resistance of the AC-based electrodes. Figure 5(b) shows the charge/discharge of the ACs/Mn3-CBs with difference current densities ranging from 0.1 to 1 A/g. The charge/discharge duration of the ACs/Mn3-CBs increases with a decrease of current density. In addition, the discharge time is longer than the charge time, which is attributed to low impurities and the interaction between the ACs/Mn-CBs and electrolyte ions.[15] And, ACs/CBs and ACs/Mn-CBs exhibit a largely ohmic drop, indicating the high equivalent series resistance (ESR) in the interface of electrodes. Although the ESR of all electrodes is high, their

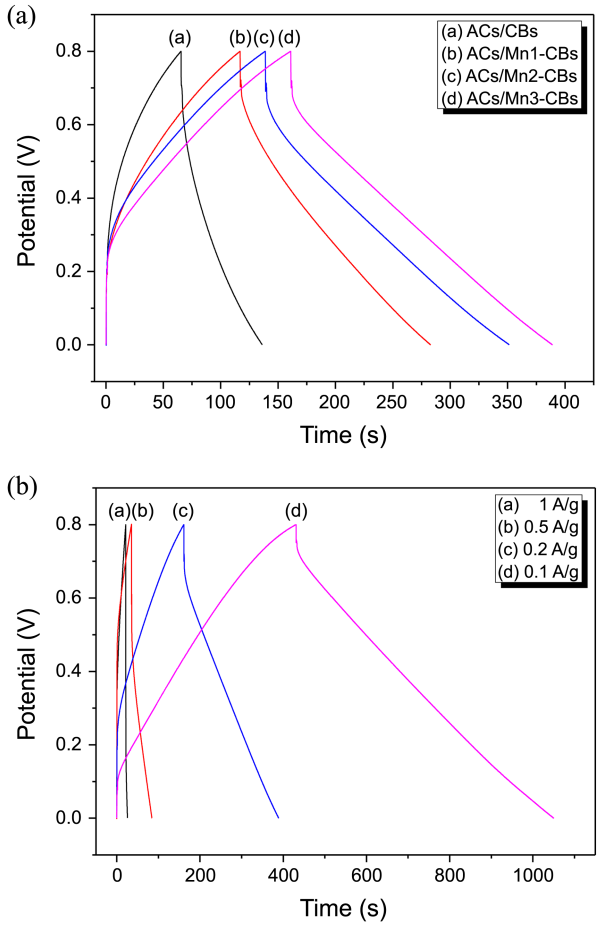


**Figure 5.** Charge-discharge curves of (a) ACs/CBs and ACs/Mn-CBs with different $Mn_3O_4$ content at 0.2 A/g current density and (b) ACs/Mn3-CBs with different current densities from 0.1 to 1 A/g.

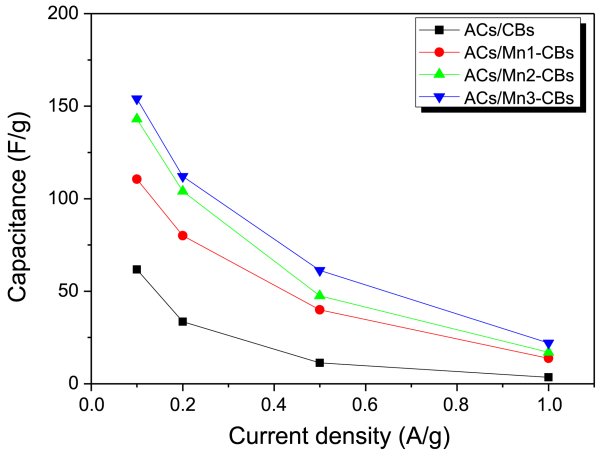


**Figure 6.** Specific capacitance of ACs/CBs and ACs/Mn-CBs with different current density from 0.1 to 1 A/g.

charge/discharge duration of ACs/Mn-CBs is significantly increased with the incorporation of $Mn_3O_4$ compared to ACs/CBs.

The specific capacitance ($C_{spec}$) for the ACs/CBs and ACs/Mn-CBs electrodes is determined from the charge-discharge curves and it can be calculated as:

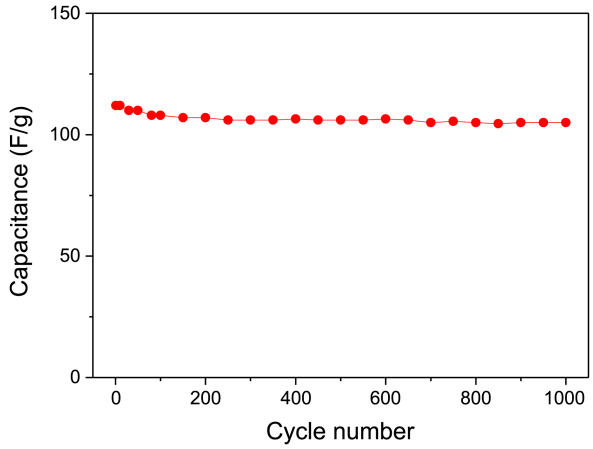


**Figure 7.** Specific capacitances of ACs/Mn3-CBs as a function of cycle number measured at 0.2 A/g current density.

$$C_{spec} = \frac{I \times t}{\Delta V \times m} \quad (1)$$

where $I$ is the discharge current, $m$ is the electrode mass, $t$ is the discharge time, and $\Delta V$ is the voltage range. As shown in Figure 6, the $C_{spec}$ of ACs/Mn-CBs electrodes is higher than that of ACs/CBs. The highest $C_{spec}$ value (154 F/g) of ACs/Mn3-CBs was obtained at 0.1 A/g current density (compared to 62 F/g for ACs/CBs, 110 F/g for ACs/Mn1-CBs, and 143 F/g for ACs/Mn2-CBs), and is attributed to the pesudocapacitance reaction of $Mn_3O_4$ incorporated into the ACs/CBs.[16] The cycle stability of ACs/Mn3-CBs is shown in Figure 7. It found that the specific capacitance was slightly decreased at the beginning of cycle. However, it kept as a constant after about 150 cycles and the specific capacitance dropped by about 6.3% after 1000 cycles, revealing an excellent cycle stability of the electrode consisted of ACs/Mn-CB.

## Conclusions

In this study, $Mn_3O_4$/carbon black (CB) composites were prepared by an *in situ* coating method as conductive fillers and the effects of the $Mn_3O_4$-CBs on the electrical performance of activated carbon (AC)-based electrodes were investigated with different $Mn_3O_4$ concentrations. Structural features of $Mn_3O_4$-CBs produced *via in situ* coating using a $KMnO_4$ solution were confirmed by XRD and TEM images, indicating the uniform coating of $Mn_3O_4$ onto the CBs. The electrical performance parameters, such as CV curves, charge-discharge behaviors, and specific capacitance of the ACs/Mn-CBs, were determined by cyclic voltammograms. ACs/Mn-CBs showed higher electrical performance than that of AC electrodes made with conventional CBs. This is attributed to the pesudocapacitance reaction of manganese oxides in the aqueous electrolyte.

**Acknowledgments.** This work was supported by the Carbon Valley Project of the Ministry of Knowledge Economy, South Korea.

## References


1. Winter, M.; Brodd, R. J. *Chem. Rev.* **2004**, *104*, 4245.
2. Pandolfo, A. G.; Hollenkamp, A. F. *J. Power Sources* **2006**, *157*, 11.
3. Ghaemi, M.; Ataherian, F.; Zolfaghari, A.; Jafari, S. M. *Electrochim. Acta* **2008**, *53*, 4607.
4. Seo, M. K.; Park, S. J. *Curr. Appli. Phys.* **2010**, *10*, 241.
5. Wu, N. L.; Wang, S. Y. *J. Power Source* **2002**, *110*, 233.
6. Hong, J. K.; Lee, J. H.; Oh, S. M. *J. Power Sources* **2002**, *111*, 90.
7. Kuroda, S.; Tobori, N.; Sakuraba, M.; Sato, Y. *J. Power Sources* **2003**, *119-121*, 924.
8. Seo, M. K.; Park, S. J. *Curr. Appli. Phys.* **2010**, *10*, 391.
9. Shinomiya, T.; Gupta, V.; Miura, N. *Electrochim. Acta* **2006**, *51*, 4412.
10. Nakayama, M.; Kanaya, T.; Inoue, R. *Electrochem. Commun.* **2007**, *9*, 1154.
11. Toupin, M.; Brousee, T.; Bélanger, D. *Chem. Mater.* **2004**, *16*, 3184.
12. Xie, X.; Gao, L. *Carbon* **2007**, *45*, 2365.
13. Huang, X.; Pan, C.; Huang, X. *Mater. Lett.* **2007**, *61*, 934.
14. Wang, Y. G.; Li, H. Q.; Xia, Y. Y. *Adv. Mater.* **2006**, *18*, 2619.
15. Wang, H.; Hao, Q.; Yang, X.; Lu, L.; Wang, X. *Electrochem. Commun.* **2009**, *11*, 1158.
16. Yan, J.; Wei, T.; Fan, Z.; Qian, W.; Zhang, M.; Shen, X.; Wei, F. *J. Power Sources* **2010**, *195*, 3041.